Available online at www.sciencedirect.com
SCIENCE DIRECT®
Acta Materialia 53 (2005) 69–77
Acta MATERIALIA
www.actamat-journals.com

Microstructures and mechanical properties of a directionally solidified NiAl–Mo eutectic alloy

H. Bei **, E.P. George *

Department of Materials Science and Engineering, University of Tennessee, 434 Dougherty Hall, Knoxville, TN 37996-2200, USA
Oak Ridge National Laboratory, Metals and Ceramics Division, 1 Bethel Valley Road, Oak Ridge, TN 37831-6093, USA

Received 8 June 2004; received in revised form 8 September 2004; accepted 11 September 2004
Available online 26 October 2004

Abstract

A NiAl–Mo ternary eutectic alloy, having the nominal composition Ni–45.5Al–9Mo (at.%), was directionally solidified in a high-temperature optical floating zone furnace. Well-aligned rod-like microstructures were obtained, consisting of NiAl matrix and 14% (by volume) continuous Mo fibers having a square cross-section. With increasing growth rate (from 20 to 80 mm/h), the spacing and size of the Mo fibers decreased, from ≈2 to 1 μm (fiber spacing) and 800 to 400 nm (fiber size). X-ray microprobe analyses revealed that the NiAl matrix contained essentially no Mo (<0.1 at.%) and had the composition Ni–45.2Al (at.%), while the composition of the Mo fibers was Mo–10.1Al–3.9Ni (at.%). From electron backscatter diffraction patterns, the following orientation relationships were obtained: $\langle 1\,0\,0\rangle_{NiAl}//\langle 1\,0\,0\rangle_{Mo}$, and $\{0\,1\,1\}_{NiAl}//\{0\,1\,1\}_{Mo}$. The growth directions and Mo/NiAl interface boundaries were found to be parallel to $\langle 1\,0\,0\rangle$ and $\{0\,1\,1\}$, respectively, in both Mo and NiAl. Nanoindentation was used to probe the mechanical properties of the individual phases in the eutectic microstructure and the modulus and hardness of the NiAl matrix were determined to be 180 and 2.9 GPa, respectively, and those of the Mo fibers 270 and 4.8 GPa. Tensile tests were used to investigate the temperature dependence of the strength and ductility of the composite. Its ductile-to-brittle transition temperature was found to be ~675 °C, and its yield strength about 25–30% higher than that of $\langle 1\,0\,0\rangle$ NiAl single crystals over the temperature range 600–1000 °C.

Keywords: Intermetallic; NiAl; Composite; Directional solidification; Eutectic microstructure; Mechanical property

1. Introduction

The ordered intermetallic compound NiAl has been investigated as a potential candidate for high temperature structural applications because of its high melting point (T_m = 1638 °C), substantially lower density (5.7 g/cm^3) than Ni-based superalloys (~8 g/cm^3), and high thermal conductivity (>6 W/m/K) [1–4]. NiAl also offers excellent oxidation resistance at temperatures above 1000 °C [5–7]. However, the use of NiAl as a structural material suffers from two major drawbacks: (a) poor ductility and fracture toughness at room temperature; and (b) low strength and creep resistance at temperatures above 600 °C.

The brittleness of NiAl at low temperatures is believed to be caused by its limited number of independent slip systems, low cleavage strength and low dislocation mobility. Some progress has been made in improving the room-temperature ductility of single-phase NiAl with the help of alloying additions and heat treatments [8–12]. Attempts have also been made to toughen NiAl by combining it with a ductile solid solution [13–23]. For example, Johnson et al. [16] showed that a

* Corresponding author. Tel.: +1 865 574 5085; fax: +1 865 576 3881.
E-mail addresses: Hbei1@utk.edu (H. Bei), georgeep@ornl.gov (E.P. George).
** Tel.: +1 865 574 4343.

1359-6454/$30.00
doi:10.1016/j.actamat.2004.09.003

room-temperature fracture toughness of ~20 MPa $\sqrt{m}$ can be achieved in a directionally solidified NiAl – 34 at.% (Cr, Mo) alloy having a fibrous or lamellar microstructure (depending on the Mo content). Similarly, Misra et al. [23] obtained a fracture toughness of ~14 MPa $\sqrt{m}$ in a NiAl – 9 at.% Mo eutectic alloy. Both these values are significantly higher than the fracture toughness of NiAl single crystal (~ 6 MPa $\sqrt{m}$, [24]).

Although the alloy investigated by Misra et al. [23] had nominally the eutectic composition, its microstructure was mostly cellular and did not consist of well-aligned Mo fibers in a NiAl matrix. This was possibly due to the relatively low temperature-gradient in their Bridgman furnace (~3 °C/mm), which may have made it difficult to maintain a planar solidification front at the growth rate employed (11 mm/h).

In the present study well-aligned microstructures of NiAl – 9 at.% Mo, devoid of any cellular or dendritic regions, were produced in a high-temperature optical floating zone furnace. This furnace has a steeper temperature-gradient (~25–33 °C/mm) [25], and has been used by us previously to produce well-aligned lamellar eutectic microstructures of Cr–Cr_3Si and V–V_3Si alloys over a wide range of growth conditions [26–29]. We report here the effects of growth conditions on the rod-like microstructures obtained in the NiAl–Mo eutectic system. We also investigated the mechanical properties of the individual phases (NiAl and Mo) by nanoindentation, and the strength and ductility of the composite by tensile testing at different temperatures.

2. Experimental procedures

2.1. Alloy preparation and directional solidification

Alloys having the nominal composition Ni–45.5Al–9Mo (at.%) were arc melted and drop cast into a cylindrical copper mold measuring 10 mm in diameter and 100 mm in length. The Ni, Al and Mo (all >99.99% pure) starting materials were carefully weighed and then mixed by arc melting, with the buttons flipped and remelted five times to ensure good mixing before drop casting. Total weight losses after melting and casting were <0.05%, which led to negligible changes in the alloy composition after melting. Therefore, all compositions discussed in this paper are nominal compositions (atomic %) unless otherwise stated.

The drop cast ingots were directionally solidified using an optical floating zone furnace. Heat from a xenon arc-lamp was focused on specimens enclosed in a quartz tube, which was first evacuated and then back filled with flowing argon gas. Drop-cast rods were used as the feed material, and pieces cut from directionally solidified rods were used as seeds. The seed rod and feed rod were rotated in opposite directions during the zone melting to form a homogeneous molten zone. The effects of growth rates on microstructures were systematically investigated by changing the growth rates from 20 to 80 mm/h at a fixed rotation rate of 60 rpm.

2.2. Metallography

The directionally solidified rods were cut transversely and longitudinally using electro-discharge machining, and representative samples were mounted in epoxy. After grinding the samples flat through 600 grit SiC paper, they were polished with diamond paste (particle size 0.5 μm) using an automatic vibratory polishing machine and etched in a solution of 80% hydrochloric and 20% nitric acids to reveal the microstructure. The etched specimens were examined by both optical and scanning electron microscopy (SEM).

2.3. Orientation relationships between the eutectic phases

Electron backscatter diffraction (EBSD) patterns were acquired in a FEI XL30 FEG SEM using an accelerating voltage of 20 kV and a 20 mm working distance. Patterns from the individual eutectic phases (NiAl and Mo) were recorded and indexed using orientation imaging microscopy (OIM). The Kikuchi-line patterns were automatically indexed by the OIM ANALYSIS package (release version 3.08, TSL™ http://www.tsl-oim.com/).

2.4. Nanoindentation

Nanoindentation experiments were conducted at 23 °C using a Nanoindenter® XP (Nano Instruments Innovation Center, MTS Corporation, Knoxville, TN). Displacements (h) and loads (P) were measured with a resolution of 0.16 nm and 0.3 μN, respectively. A Berkovich diamond indenter (3-sided pyramidal tip) was used. The area function of the tip and the compliance of the nanoindentation system were calibrated by testing fused quartz standard specimens using the method of Oliver and Pharr [30]. The continuous stiffness measurement mode was used for all the experiments. The experiments were run in load control at a constant loading rate $\dot{P}/P = 0.03\ s^{-1}$ to a prescribed maximum load of 3 mN.

2.5. Tensile tests

Dogbone-shape tensile specimens with gage sections measuring $2 \times 2 \times 10$ mm were electro-discharge machined from the directionally solidified rods. The surfaces of the gage section were ground through 600 grit SiC paper to eliminate any micro-cracks that may have formed during electro-discharge machining. Tensile tests were conducted on a screw-driven Instron machine equipped with a vacuum chamber and induction heater.

The chamber was first evacuated to a vacuum better than 8×10^{-6} Torr, and then the specimens were heated to the test temperature (which varied from room temperature to 1000 °C). All the specimens were tested at a constant cross head displacement rate of 2.54 mm/min, which corresponds to an engineering strain rate of 4.2×10^{-3} s^{-1}. The specimen lengths before and after fracture were measured to calculate the percent elongation to fracture (assuming that all the strain occurred in the gage section). Yield strengths were calculated using the 0.2% offset method. Fracture surfaces were examined in a SEM.

3. Results and discussion

3.1. Microstructures

Fig. 1 shows the typical rod-like microstructure of the directionally solidified NiAl–Mo eutectics grown in this study. For a range of solidification conditions (growth rates from 20 to 80 mm/h at a fixed rotation rate of 60 rpm), a well-aligned rod-like structure was observed throughout the cross sections of the specimens (~8 mm in diameter) except for a narrow rim (about 1-mm thick) near the outer surface of the specimen where the microstructure was misaligned. This surface effect is most likely caused by quenching from the continuous argon flow during directional solidification. In the transverse and longitudinal sections shown in Fig. 1, the NiAl phase is the matrix and the Mo phase the continuous fibers.

The arrangement of the Mo rods in the transverse section is approximately hexagonal (Fig. 1(c)). As shown in Fig. 1(d), if circles having equal radii are drawn around the Mo fibers during steady-state growth from the melt, a hexagonal pattern naturally results at the points where the circles intersect with each intersection point being equidistant from its neighbors. The size of the circles is determined by the diffusion distance, which in turn is determined by the time available for diffusion (or the directional solidification rate); i.e., the faster the growth rate, the smaller the circles and hence the fiber spacing. But the size of the diffusion zone around each Mo fiber is the same (for a given growth rate); i.e., all the circles have the same radius. Therefore, as the solidification rate changes, although the pattern will get tighter or more open, it remains essentially hexagonal (except for growth faults, Fig. 1(a)). It is interesting to note that the shape of the individual Mo rods in the transverse section is square rather than circular (Fig. 1(c)), suggesting that the NiAl–Mo interfacial energy is highly anisotropic.

X-ray microprobe analysis was conducted to determine the compositions of these two phases. It was found that NiAl matrix contained essentially no Mo (<0.1%) and had the off-stoichiometric composition Ni–45.2Al, whereas the Mo fibers contained all three

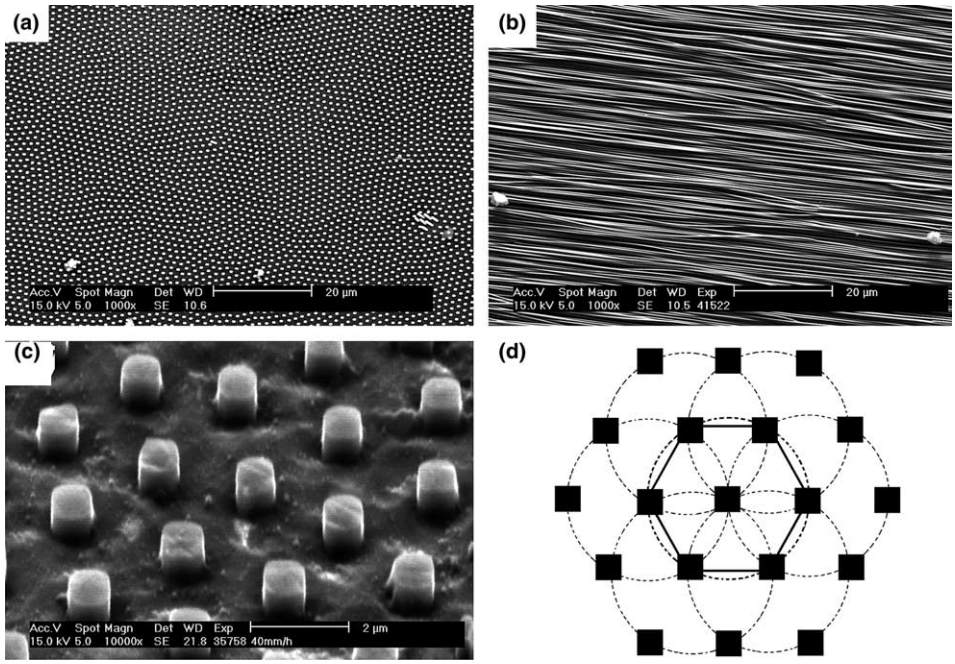

Fig. 1. SEM micrographs showing well-aligned rod-like microstructure of the NiAl–Mo eutectic alloy directionally solidified at 40 mm/h and 60 rpm with the NiAl matrix preferentially etched: (a) transverse section; (b) longitudinal section; (c) higher magnification view of transverse section showing that the cross sections of the Mo fibers have a square rather than circular shape; (d) schematic diagram showing that a hexagonal pattern naturally results at the intersections of equal-radius circles drawn around the Mo fibers.

elements and had the composition Mo–10.1Al–3.9Ni. The volume fraction of the Mo phase was measured and found to be 14.1%. From the chemical compositions, densities and volume fractions of the eutectic phases (and using the lever rule in the NiAl–Mo pseudo-binary phase diagram), the eutectic composition of this alloy was calculated to be Ni–43Al–10Mo, which is slightly different from our nominal alloy composition (Ni–45.5Al–9Mo). This discrepancy is not due to a change in alloy composition during processing since there was negligible weight loss during melting or directional solidification.

A possible reason for the discrepancy is that we used the density of pure Mo in the above calculation. Attempts to arc melt an alloy having the fiber composition (Mo–10.1Al–3.9Ni) and determine its density were unsuccessful because the high melting point of Mo (2610 °C) resulted in excessive Al evaporation. Another possibility is that the alloy compositions used in this and previous studies [23], are not in fact the eutectic composition. As discussed in an earlier paper [26], even off-eutectic compositions can produce structures that look eutectic if the temperature gradient is high enough and the growth rate slow enough, i.e., if a stable, planar solid/liquid interface can be maintained during directional solidification. According to the theory of constitutional supercooling, the growth condition for producing such an interface, in the absence of convection, is

$$\frac{G_L}{R} \geqslant -\frac{m_L(C_E - C_0)}{D}, \quad (1)$$

where G_L is the temperature gradient in the liquid ahead of the interface, R is the growth rate, m_L is the slope of the liquidus, C_E is the eutectic composition, C_0 is the initial composition of the solidifying alloy, and D is the inter-diffusion coefficient [31,32]. All the parameters on the right hand side of Eq. (1) are material constants; therefore, the left hand side predicts that, for a given growth rate, a large temperature gradient favors the formation of a fully eutectic structure. This may explain why cellular microstructures were previously obtained when the temperature gradient was small (~3 °C/mm) [23] whereas well-aligned fully eutectic microstructures are obtained here when the temperature gradient is 10 times higher (25–33 °C/mm) even though both studies investigated nominally the same alloy composition.

Another point to note is that alloys on the NiAl side of the eutectic composition in the pseudo-binary NiAl–Mo system should more easily form fully eutectic structures, than those on the Mo-rich side. This is because the melting points of NiAl and Mo are ~1638 and 2620 °C, respectively [33], and the eutectic temperature is ~1600 °C [34], which results in a smaller slope of the liquidus (m_L) on the NiAl-rich side than on the Mo-rich side, which in turn makes the right hand side of Eq. (1) smaller.

3.2. Crystallographic orientation relations

Orientation imaging microscopy was used to determine the crystallographic orientations of the two eutectic phases (NiAl and Mo) and their interfacial planes. Specimens directionally solidified at 40 mm/h and 60 rpm were examined (microstructure shown in Fig. 1). EBSD patterns were recorded from the individual phases at different locations within the as-grown composite. Fig. 2 shows the EBSD patterns from the NiAl matrix and the Mo rods. The NiAl–Mo interface boundaries were determined to be parallel to the {0 1 1} planes in both NiAl and Mo. In addition, the growth direction was found to be parallel to the ⟨1 0 0⟩ directions in both NiAl and Mo. Fig. 3 schematically summarizes these crystallographic orientation relationships.

The {0 1 1} interface boundary planes observed in this study are in agreement with those reported previously [23]. These are the closest-packed planes in the BCC and B2 crystal structures of Mo and NiAl [35], respectively. During eutectic growth such high-density planes are probably selected as inter-phase boundaries to minimize the boundary energies (which is also consistent with the Mo fibers having a square rather than a circular shape). The ratio of the lattice parameters of Mo and NiAl is about 1.09 [35], indicating that the interface between the NiAl matrix and Mo fibers is probably incoherent (or semi-coherent).

The growth directions observed in this study, namely ⟨1 0 0⟩ in both NiAl and Mo, are not the same as those reported in an earlier study [23] where they were found to deviate by ~15–20° from ⟨1 0 0⟩. A possible reason for this difference is the well-aligned microstructure obtained in this study compared to the cellular microstructure observed earlier [23]. When the microstructure is well-aligned, all the Mo fibers are normal to the transverse section (on which the microstructural observations are made). In contrast, the Mo fibers in the cellular structures intersect the transverse section at different angles making it difficult to unambiguously determine the growth direction.

3.3. Effects of growth rate on microstructure

The fiber spacing, defined as the average distance on a transverse section between the centers of adjacent Mo fibers (λ in Fig. 3), and the fiber size, defined as the average edge length of the square cross-sections (a in Fig. 3), were measured over a range of growth rates, R, from 20 to 80 mm/h at a fixed rotation rate of 60 rpm. Fig. 4(a) and (b) shows examples of the typical microstructures obtained at growth rates of 20 and 80 mm/h. When the growth rate decreased from 80 to 20 mm/h, the fiber spacing increased from ~1100 to ~2200 nm and the fiber size from ~370 to ~750 nm.

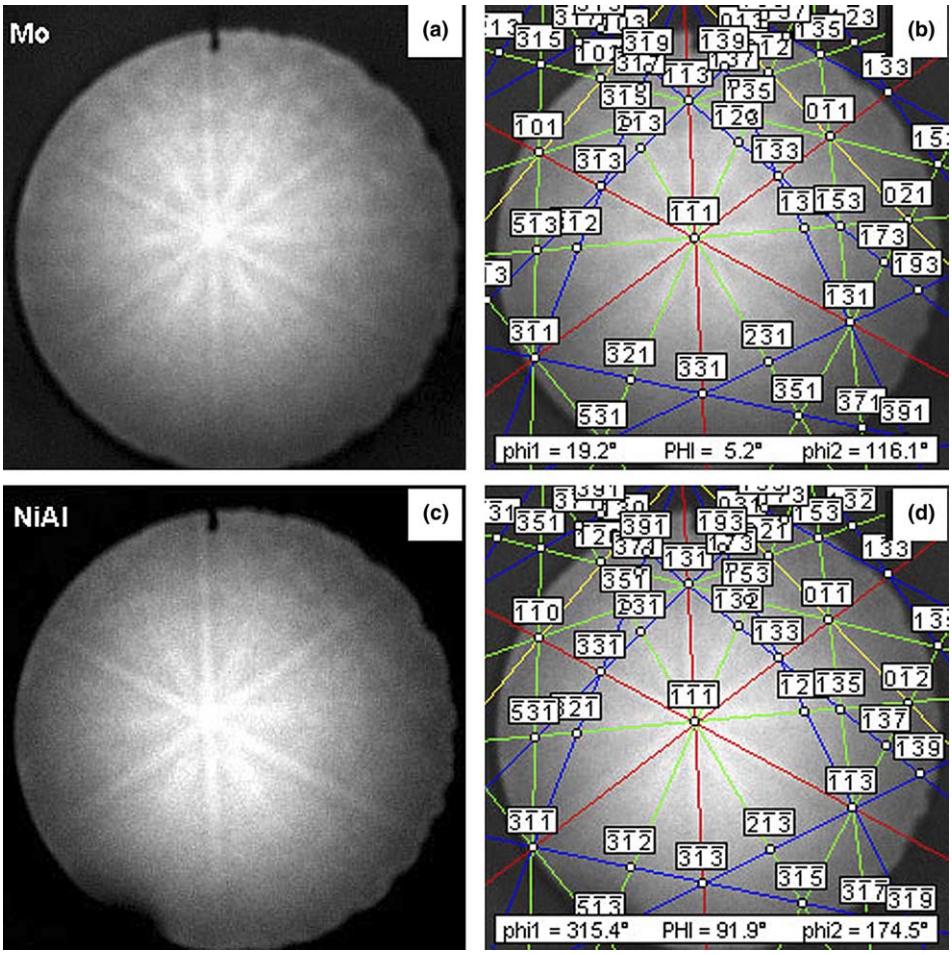

Fig. 2. Electron backscatter diffraction (EBSD) patterns obtained from (a) Mo fibers and (c) NiAl matrix, on a transverse section of the directionally solidified NiAl–Mo eutectic alloy; (b) and (d) are indexed EBSD patterns of (a) and (c). These images were obtained with the normal direction (ND) at 70° to the electron beam direction.

Jackson and Hunt [36] obtained the following relationship between growth rate R and spacing λ by considering the balance between the diffusion required for phase separation and the energy required for interphase boundary formation:

$$\lambda^2 R = \frac{a^{\mathrm{R}}}{Q^{\mathrm{R}}} = C_1, \tag{2}$$

where Q^{R} and a^{R} (and C_1) are constants related to the magnitudes of the liquidus slopes at the eutectic temperature, the composition difference between the two phases, their volume fractions, the solid–liquid interface energies of two phases, and the liquid–solid interface shape. In the present study, C_1 is assumed to have a fixed value over the range of experimental conditions investigated.

An expression similar to the one above can be derived also for the relationship between fiber size (a) and growth rate (R), as shown below. Since the fiber arrangement in the transverse section is hexagonal, the fiber size (a) is related to the fiber spacing (λ) and the volume fraction of the fibers (V_{f}) by

$$a^2 = \tfrac{\sqrt{3}}{2} V_{\mathrm{f}} \lambda^2, \tag{3}$$

where V_{f} is constant for a given alloy composition. It is possible to eliminate λ from Eqs. (2) and (3) and obtain the following relationship between fiber size and growth rate:

$$a^2 R = C_2. \tag{4}$$

where C_2 is another constant. From Eqs. (2) and (3) it is seen that both fiber size and spacing are expected to vary inversely as the square root of growth rate.

Fig. 5 is a plot of the measured values of λ and a as a function of growth rate R. As can be seen in this figure, the data lie reasonably well on straight lines drawn through the origin when λ and a are plotted against the reciprocal of the square root of the growth rate, $R^{-1/2}$. The relations between R and λ, and R and a can be written as:

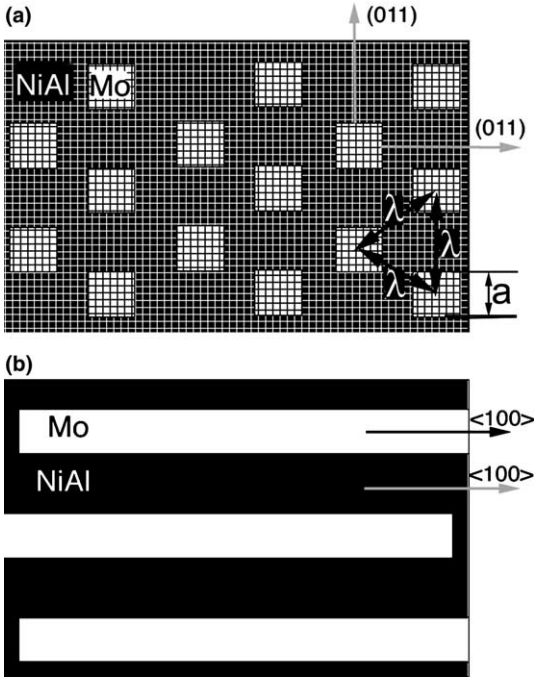

Fig. 3. Schematic diagrams showing the observed crystallographic orientation relationships between the NiAl matrix and Mo fibers in directional solidified NiAl–Mo eutectics: (a) transverse; (b) longitudinal sections. The parameters λ and a refer to fiber spacing and size, respectively.

$$\lambda R^{1/2} = 9.76\ \mu\text{m mm}^{1/2}/\text{h}^{1/2},$$
$$aR^{1/2} = 3.42\ \mu\text{m mm}^{1/2}/\text{h}^{1/2}. \quad (5)$$

From Eq. (5), the ratio of fiber spacing to size, λ/a, is found to be 2.85. When this value is substituted into Eq. (3), the volume fraction of Mo fibers is calculated to be 14.2%, which is in excellent agreement with the measured value of 14.1%.

3.4. Hardness and modulus

The hardness and modulus of the individual phases in directionally solidified NiAl–Mo were measured by nanoindentation using a maximum load of 3 mN. Several of the indents fell entirely within one or the other of the two phases. Fig. 6 shows two examples of such indents, one located in the NiAl matrix (Fig. 6(a)), and another in the Mo fiber (Fig. 6(b)). Using such indents, the indentation hardnesses were determined to be 4.8 ± 0.4 GPa for the Mo phase and 2.9 ± 0.2 GPa for the NiAl phase.

The modulus was calculated from continuous stiffness measurements using the method of Oliver and Pharr [30]. Poisson's ratio of 0.3 was used in all the calculations. The modulus of the Mo phase was found to be 270 ± 11 GPa and that of the NiAl matrix 180 ± 8 GPa. Because both NiAl and Mo are elastically anisotropic, the nanoindentation modulus along specific directions (e.g., $\langle 100 \rangle$ here) obtained using the Oliver–Pharr method cannot be directly compared to the directional Young's modulus (e.g., E_{100}). Rather, the

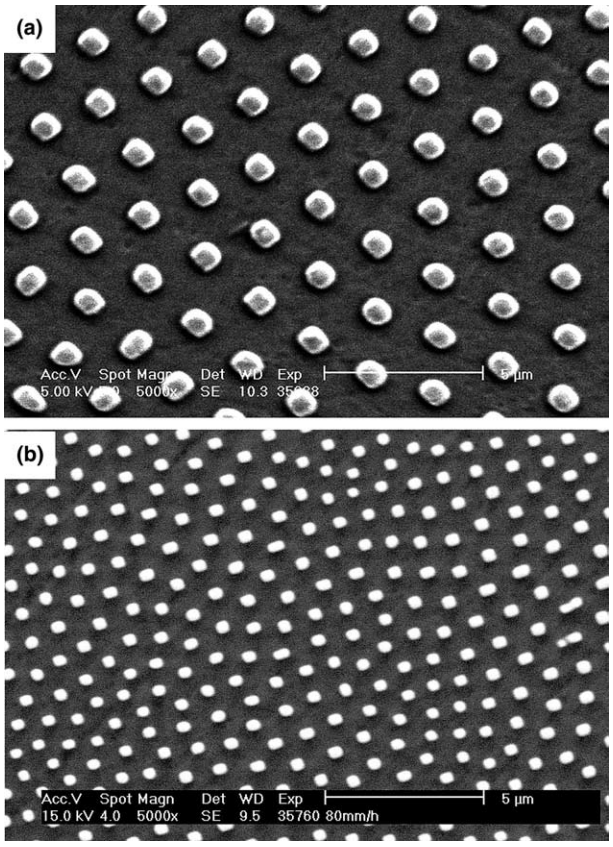

Fig. 4. SEM micrographs showing (a) coarse (20 mm/h growth rate), and (b) fine (80 mm/h growth rate) rod-like microstructures in directionally solidified NiAl–Mo alloys. The rotation rate was fixed at 60 rpm.

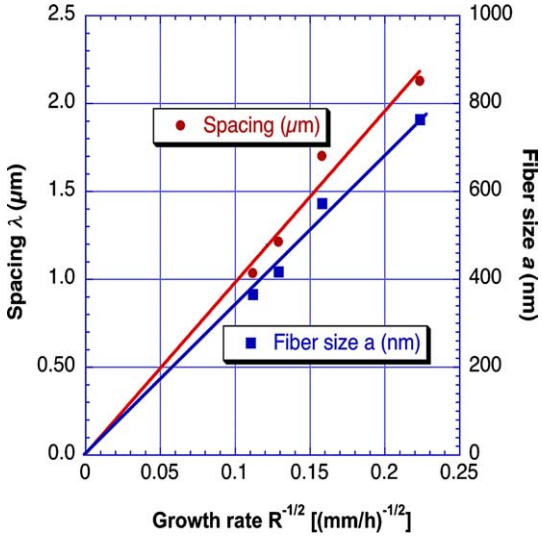

Fig. 5. Effects of growth rate on Mo fiber spacing and size in directionally solidified NiAl–Mo alloys at a fixed rotation rate of 60 rpm.

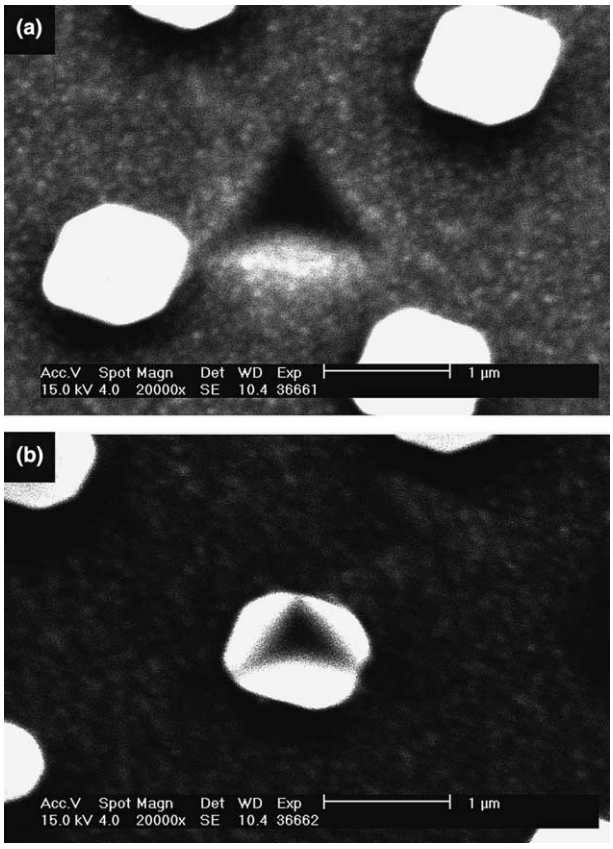

Fig. 6. Micrographs showing examples of nanoindentation impressions in a NiAl–Mo eutectic alloy directionally solidified at 20 mm/h and 60 rpm: (a) an indent lying entirely within the NiAl phase; (b) an indent lying entirely within the Mo phase.

modulus obtained from nanoindentation is some polycrystalline average of the anisotropic elastic constants. Vlassak and Nix [37,38] showed that, for a material with cubic symmetry, the modulus obtained by indentation on a (hkl) surface of a single crystal can be written as the product of a correction factor and the modulus of an isotropic, randomly oriented, polycrystalline aggregate of the same material. If elastic constants of a Ni–45Al single crystal [39] are used in the Vlassak and Nix formula, the calculated modulus for indentation on the {1 0 0} plane of the NiAl phase is 182 GPa, which is close to the value measured here (180 GPa). However, for the Mo phase in our composite, the modulus calculated from the elastic constants of a Mo single crystal [40] is 352 GPa, which is 23% larger than our experimental value (270 GPa). There are two possible reasons for this discrepancy. First, because the size of the Mo phase is quite small (less than 1 μm) there may be some influence of the surrounding NiAl matrix, which has a significantly lower modulus. Second, the Mo phase in the composite is not pure Mo, but rather contains about 10.1% Al and 3.9% Ni, which probably lower the modulus. As mentioned before, we were unsuccessful in producing a single-phase Mo alloy having the composition of the fibers (because of excessive Al evaporation) and, therefore, could not verify this latter possibility.

3.5. Tensile properties

Tensile tests at room temperature and various elevated temperatures were conducted to investigate the mechanical properties of the NiAl–Mo composite directionally solidified at 80 mm/h and 60 rpm (microstructure shown in Fig. 4(b)). The tensile loads were applied parallel to the growth direction, i.e., parallel to the Mo fibers. At room temperature the alloy broke in a brittle manner without prior yielding but at temperatures $\geqslant$600 °C, yielding was clearly observed. Fig. 7 is a plot of the 0.2% off-set yield strength, ultimate tensile strength (UTS), and ductility (represented by percent elongation to fracture) as a function of temperature. The yield strength decreases continuously, from 487 to 209 MPa, as the temperature is increased from 600 to 1000 °C; at the same time, the elongation to fracture increases from ~4% to 28%. Between 650 and 700 °C, the ductility increases sharply from ~4% to 25%. Therefore, the ductile-to-brittle transition temperature for this material lies somewhere between 650 and 700 °C. The temperature dependence of the yield strength of ⟨1 0 0⟩-oriented NiAl single crystals [41] is shown in Fig. 7 for comparison (this is the same orientation as that of the NiAl matrix in our composite). Over the entire temperature range, the NiAl–Mo composite is stronger than monolithic NiAl by ~25–30%.

When compared to NiAl single crystals, NiAl–Mo composites have two main advantages: increased fracture toughness at room temperature, as shown by Misra et al. [23], and better high-temperature strength, as

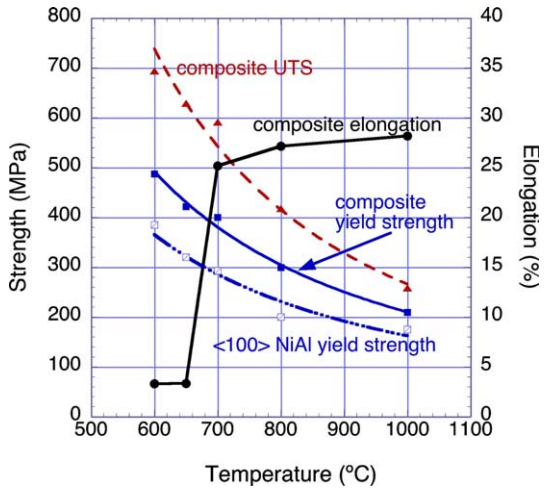

Fig. 7. Yield strength, ultimate tensile strength (UTS) and ductility (% elongation to fracture) as a function of temperature in directionally solidified NiAl–Mo alloys. The temperature dependence of the yield strength [41] of ⟨1 0 0⟩ NiAl single crystals (same orientation as the NiAl matrix in the composites) is included for comparison.

shown here. But our NiAl–Mo composite has the disadvantage that its brittle-to-ductile transition temperature (~675 °C) is higher than that of a stoichiometric NiAl {1 0 0} single crystal, ~375 °C [41].

Fracture surfaces after tensile testing were examined by SEM. Fig. 8(a)–(c) shows the fracture surfaces of NiAl–Mo alloys after tensile testing at room temperature, 600 and 800 °C, respectively. At temperatures below the brittle–ductile transition temperature (~675 °C), there is smooth cleavage in the NiAl matrix, and debonding of the NiAl–Mo interface accompanied by fiber pull-out (Fig. 8(b)), suggesting that the NiAl phase is brittle and the NiAl/Mo interface weak at these temperatures. However, the Mo solid-solution phase is ductile and exhibits limited necking even at room temperature (Fig. 8(a)). At 600 °C, which is below the brittle–ductile transition temperature of the overall composite, the Mo fibers exhibit extensive ductility and necking (almost to a point), whereas the NiAl matrix remains relatively brittle (Fig. 8(b)). With increasing temperature (>700 °C), the fracture surface of the NiAl matrix becomes rough and shows evidence of increased plastic deformation (Fig. 8(c)). At these temperatures, only slight debonding of the NiAl/Mo interface is observed, suggesting that the NiAl matrix and Mo fibers deform together (as shown in the inset of Fig. 8(c)). After the specimens fractured at 800 °C, the reduced area of the fracture surface was found to be about 75% of the initial area. This necking appears to be accommodated by chisel-edge flow in the Mo fibers resulting in their elongated (rectangular) shape on the fracture surface.

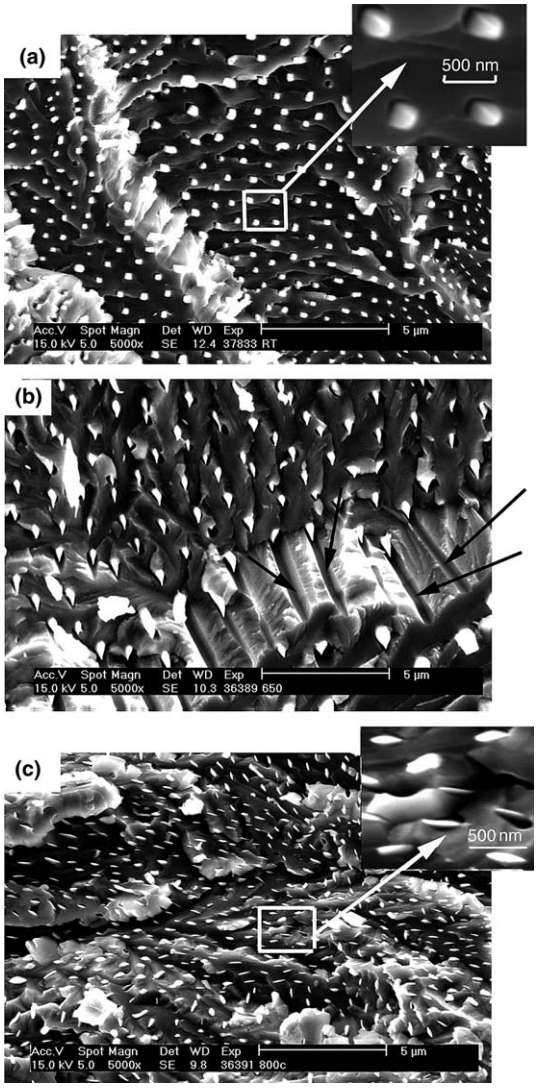

Fig. 8. Fracture surfaces after tensile testing in vacuum at: (a) room temperature; (b) 600 °C; (c) 800 °C. The arrows in (b) show grooves in the NiAl matrix where fiber pull-out occurred.

4. Conclusions

Directional solidification in an optical floating zone furnace was used to produce well-aligned rod-like microstructures of NiAl–Mo eutectic alloys. The structures consist of 14 vol% Mo (solid-solution) fibers having a square cross section embedded in an intermetallic NiAl matrix. The composition of the fibers is Mo–10.1Al–3.9Ni and that of the matrix Ni–45.2Al (<0.1 Mo).

The growth direction is ⟨1 0 0⟩ in both the NiAl matrix and the Mo fibers, and the NiAl/Mo interface boundaries are parallel to the {0 1 1} planes in both phases.

Both fiber spacing (λ) and size (a) decrease inversely as the square root of the growth rate (R), i.e., $\lambda \propto R^{-1/2}$ and $a \propto R^{-1/2}$. Fiber spacings range from ~1 to 2 μm and fiber sizes from ~400 to 800 nm for growth rates ranging from 80 to 20 mm/h.

The nanoindentation modulus and hardness of the NiAl matrix are 180 and 2.9 GPa, and those of the Mo fibers 270 and 4.8 GPa. At room temperature, the NiAl–Mo composite breaks in a brittle manner before yielding. With increasing temperature (from 600 to 1000 °C), its ductility increases (from ~4% to 28% elongation to fracture), while tensile strength decreases (from 487 to 209 MPa). When compared to ⟨1 0 0⟩ NiAl single crystals the yield strength of the NiAl–Mo composite is 25–30% higher at temperatures in the range 600–1000 °C.

Acknowledgements

This research was sponsored by the Division of Materials Sciences and Engineering, Office of Basic Energy Sciences, US Department of Energy, and the SHaRE Collaborative Research Center at Oak Ridge National Laboratory, under contract DE-AC05-00OR22725 with UT-Battelle, LLC. The authors thank Larry Walker of ORNL for help with the X-ray microprobe analysis.

References

[1] Liu CT. Mater Chem Phys 1996;42:77.
[2] Noebe RD, Bowman RR, Nathal MV. Int Mater Rev 1993;38:193.
[3] Miracle DB. Acta Metall 1993;41:649.
[4] George EP, Liu CT. J Mater Res 1990;5:754.
[5] Barrett CL. Oxid Met 1988;30:361.
[6] Smialek JL, Meier GH. In: Sims CT, Stoloff NS, Hagel WC, editors. Superalloys II. Chichester: Wiley; 1987. p. 293.
[7] Doychak J, Smialek JL, Barrett CA. In: Grobstein T, Doychak J, editors. Oxidation of high temperature intermetallics. Warrendale: TMS; 1989. p. 41.
[8] Darolia R. J Met 1991;43:44.
[9] Hack JE, Brzeski JM, Darolia R. Scr Metall 1992;27:1259.
[10] Weaver ML, Noebe RD, Lewandowski JJ, Oliver BF, Kaufman MJ. Mater Sci Eng A 1995;93:179.
[11] Liu CT, Lee EH, George EP, Duncan AJ. Scr Metall 1994;30:387.
[12] Darolia R, Lahrman DF, Field RD. Scr Metall 1992;26:1007.
[13] Misra A, Wu ZL, Kush MT, Gibala R. Mater Sci Eng A 1997;239–240:75.
[14] Subramanian PR, Mendiratta MG, Miracle DB. Metall Mater Trans A 1994;25:2769.
[15] Joslin SM, Chen XF, Oliver BF, Noebe RD. Mater Sci Eng A 1995;196:9.
[16] Johnson DR, Chen XF, Oliver BF, Noebe RD, Whittenberger JD. Intermetallics 1995;3:99.
[17] Cline HE, Walter JL, Lifshin E, Russell RR. Metall Trans 1971;2:189.
[18] Subramanian R, Mendiratta MG, Miracle DB, Dimiduk DM. In: Anton DL, Martin PL, Miracle DB, McMeeking R, editors. Intermetallic matrix composites. Pittsburgh: Materials Research Society; 1990. p. 147.
[19] Frommeyer G, Rahlbauer R. In: George EP, Inui H, Mills MJ, Eggeler G, editors. Defect properties and related phenomena in intermetallic alloys. Warrendale: Materials Research Society; 2003. p. 193.
[20] Milenkovic S, Caram R. Mater Lett 2002;55:126.
[21] Milenkovic S, Coelho AA, Caram R. J Crystallogr Growth 2000;211:485.
[22] Walter JL, Cline HE. Metall Trans 1970;1:1221.
[23] Misra A, Wu ZL, Kush MT, Gibala R. Philos Mag A 1998;78:533.
[24] Chang KM, Darolia R, Lipsitt HA. Acta Metall Mater 1992;40:2722.
[25] Hirano T. National Institute for Materials Science, Japan, private communication.
[26] Bei H, George EP, Kenik EA, Pharr GM. Acta Metall 2003;51:6241.
[27] Bei H, George EP, Pharr GM. Intermetallics 2003;11:283.
[28] Bei H, George EP, Kenik EA, Pharr GM. Z Metallkunde 2004;95:505.
[29] George EP, Bei H, Serin K, Pharr GM. Mater Sci Forum 2003;426–432:4579.
[30] Oliver WC, Pharr GM. J Mater Res 1992;7:1564.
[31] Tiller WA. Liquid metals and solidification. Cleveland: American Society for Metals; 1958.
[32] Flemings MC. Solidification processing. New York: McGraw-Hill, Inc; 1974.
[33] Massalski TB, editor. Binary alloy phase diagram. Metals Park: American Society for Metals; 1987.
[34] Maslenkov SB, Udovskii AL, Burova NN, Rodimkina VA. Izv Akad Nauk SSSR, Met 1986;1:198.
[35] Villars P, Calvert LD. Pearson's handbook of crystallographic data for intermetallic phases. Metals Park: American Society for Metals; 1985.
[36] Jackson KA, Hunt JD. Trans Metall Soc AIME 1966;236:1129.
[37] Vlassak JJ, Nix WD. J Mech Phys Solid 1994;4:1223.
[38] Vlassak JJ, Nix WD. Philos Mag A 1993;67:1045.
[39] Rusovic N, Warlimont H. Phys Stat Sol A 1977;44:609.
[40] Simmons G, Wang H. Single crystal elastic constants and calculated aggregated properties: a handbook. Cambridge: The MIT Press; 1971.
[41] Field RD, Lahrman DF, Darolia R. Acta Metall Mater 1991;39:2951.